

Pilot Study on the Measurement of the Production of Boron Isotopes in C+p Reactions at 13.5A GeV/c with NA61/SHINE

Neeraj Amin* for the NA61/SHINE collaboration

Karlsruhe Institute of Technology , Institute for Astroparticle Physics, Karlsruhe, Germany

E-mail: neeraj.amin@kit.edu

The current understanding of cosmic-ray propagation in the Galaxy is significantly hindered by the inadequate knowledge of nuclear fragmentation cross-sections, while the other key component, the secondary cosmic-ray fluxes are measured with high precision by space-based detectors. This situation can be redressed by utilizing NA61/SHINE, a fixed-target experimental facility at CERN. Pilot data on fragmentation was taken in the year 2018 with the main goal of probing the feasibility of performing fragmentation studies at SPS energies. Two fixed targets, polyethylene (C₂H₄) and graphite were employed to study C+p interactions at 13.5A GeV/c beam momentum. In this contribution, we will present the preliminary measurement of the direct production of isotopes of boron ¹⁰B and ¹¹B in C+p interactions at NA61/SHINE.

38th International Cosmic Ray Conference (ICRC2023)
26 July – 3 August 2023
Nagoya, Japan



*Speaker

1. Introduction

Modeling the secondary-to-primary flux ratios of cosmic rays at Earth, such as the Boron-to-Carbon flux ratio, allows to constrain the cosmic-ray (CR) propagation in the Galaxy. Recently, space-based particle detectors like AMS-02 and CALET have made significant advancements in measuring the ratio of secondary-to-primary galactic cosmic rays (GCRs) with a precision of $<5\%$ at energies of around $10A$ GeV [1–4]. However, the lack of comprehensive knowledge regarding nuclear fragmentation cross-sections, especially at these energies, imposes limitations on the accuracy of CR propagation calculations, leading to uncertainties of up to 20% (e.g. Refs. [5, 6]).

Since current cosmic-ray measurements encompass energies up to several hundreds of GeV, it becomes crucial to enhance the precision of laboratory measurements of the fragmentation cross-section above $10A$ GeV/ c . Doing so will help reduce uncertainties in GCR propagation models. One essential process for evaluating CR propagation is the fragmentation of primary CR carbon (^{12}C) into boron (^{11}B and ^{10}B) when interacting with the interstellar medium primarily composed of protons. The B-to-C flux ratio is the most widely studied and measured quantity for propagation characteristics. Pilot run measurements with NA61/SHINE reported previously include the direct total boron production with NA61/SHINE [7], and the supplementary contribution to B-production in the Galaxy arising from the unstable ^{11}C [8]. In this work, we report on the production of the boron isotopes ^{11}B & ^{10}B in $^{12}\text{C}+p$ interactions at a beam momentum of $13.5A$ GeV/ c .

The details of the NA61/SHINE experimental facility are given in Section 2. In Section 3.1, we describe the methodology of fragmentation measurements conducted at NA61/SHINE and Section 3.2 explains the cross-section calculation framework. We conclude with the preliminary results of the production of boron isotopes in Section 4.

2. NA61/SHINE

Situated in the North Area at the H2 beam-line of the CERN Super Proton Synchrotron (SPS), the NA61/SHINE (SPS Heavy Ion and Neutrino Experiment) is a fixed target facility that serves as a versatile, multi-purpose experiment [9]. Its primary objective is to investigate the characteristics of hadron production in nuclear interactions using fixed targets at SPS energies. The facility presents a unique opportunity to study the production of light secondary nuclei, such as Li, Be, and B, by examining the fragmentation of light nuclei like C, N, and O, which is relevant to the propagation of GCRs [6]. To achieve this, a primary ^{208}Pb ion beam from the SPS is directed to collide with the primary 16 cm long T2 beryllium target located on the H2 beam line. As a result of this, the Pb nucleus fragments into lighter secondary nuclei. These nuclei are further selected based on their rigidity and transported to the NA61/SHINE facility.

The basic layout of the NA61/SHINE facility during the 2018 pilot run is shown in Fig. 1. The A-det is the most upstream detector. It is a 6×6 cm² plastic scintillator located ~ 240 m upstream of the S1 scintillator, which is of similar dimensions. The time-of-flight of the beam nuclei between the A and S1 detectors identifies the incoming isotopes. The three Beam Position Detectors (BPDs) along with veto scintillators (V^0 , V^1 & V^{1P}) located upstream of the target are used to characterize the beam based on its composition and angular spread. The beam trigger is defined with the signals from the scintillators S1 and the veto detectors. On the downstream side of the target, the primary

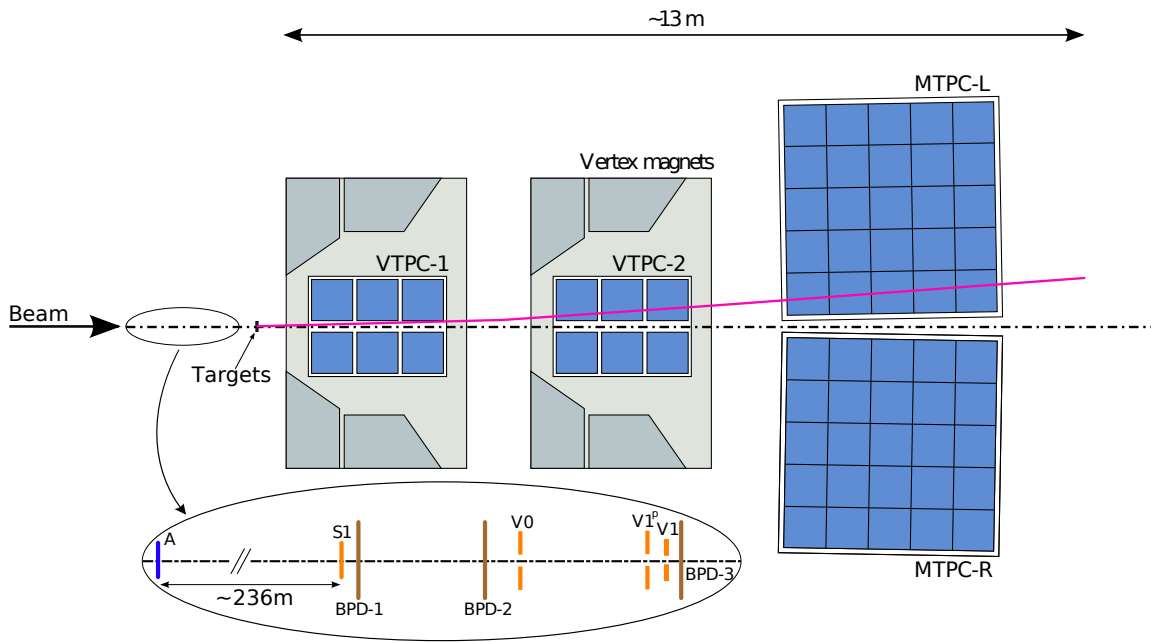


Figure 1: The NA61/SHINE detector layout. The inset shows the A-S1 system used for time-of-flight tagging of isotopes and other beam-line detectors upstream of the target, during the pilot run on fragmentation.

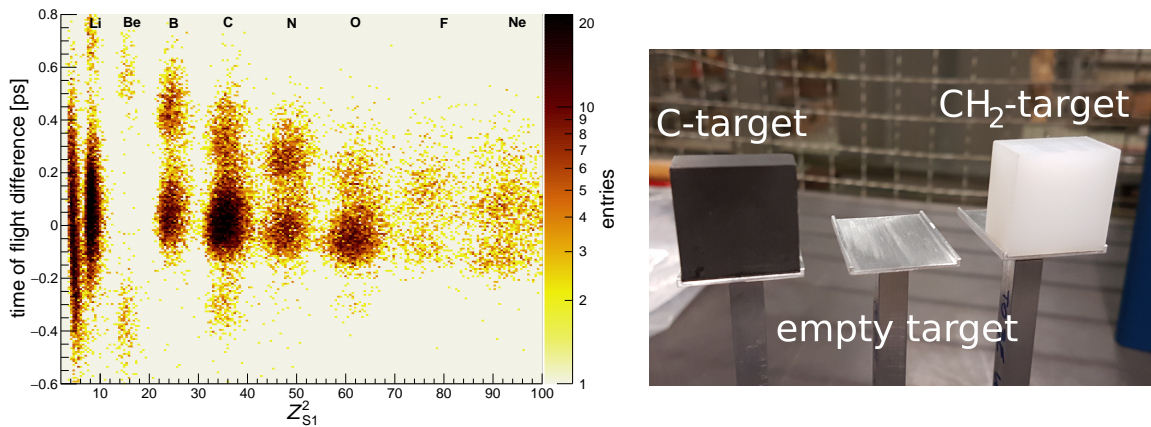


Figure 2: Left: The time-of-flight vs. squared charge signal from the S1 scintillator for the secondary nuclei resulting from fragmentation of the ^{208}Pb nucleus. Right: The target-holder with the PE and C targets.

sub-detectors used for the measurements are the time projection chambers (TPCs). As seen in Fig. 1, the Vertex TPCs 1&2 are placed inside a super-conducting magnet with a total bending power of 9 Tm. Following the VTPCs are two Main TPCs (MTPCs) used as the primary detector for measuring the produced fragments.

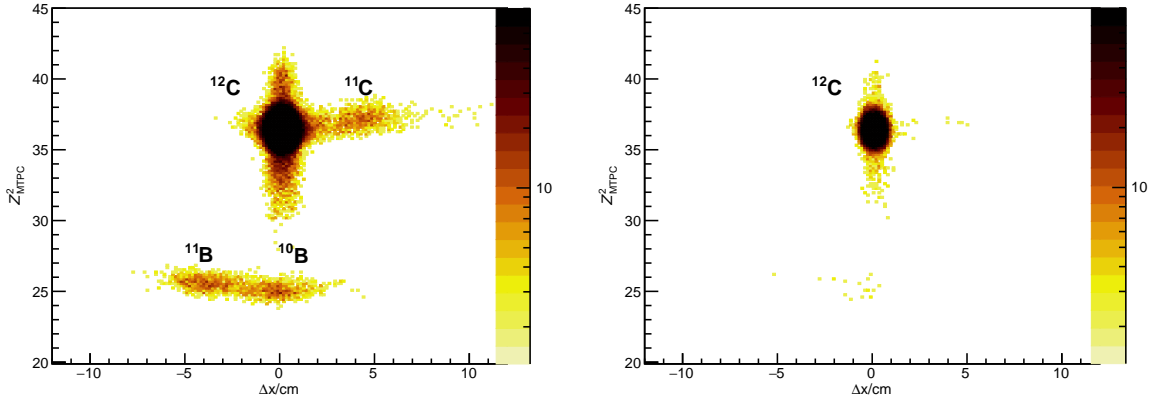


Figure 3: The 2D-distribution of fragments as seen in the MTPC-L for the target-IN (*left*) and target-OUT (*right*) case. The non-interacting ^{12}C beam particles are seen as the dark blob at $\Delta x = 0.0$ cm with lighter fragments on either side of it depending on their rigidity relative to the beam rigidity.

3. Measurement with NA61/SHINE

3.1 Pilot Run on Fragmentation

In order to study the feasibility of measuring nuclear fragmentation cross-sections, a dedicated pilot run was conducted in December 2018, recording $\sim 10^6$ events over the period of 3 days of data-taking [10]. The primary goal of this run was to measure the total boron production from $^{12}\text{C}+p$ interactions at a beam momentum of $13.5A$ GeV/ c . As mentioned in Section 2, the secondary ion beam for this run was produced by impinging the primary Pb ion beam on a 16 cm long beryllium target. This target was chosen to maximize the ^{12}C fragment yield. The collimators and spectrometers on the H2 beam line were tuned to select nuclei with $A/Z = 2$ at a beam momentum of $13.5A$ GeV/ c . The time-of-flight measured between the two scintillators A and S1, separated by ~ 240 m, and the energy deposited in the S1 scintillator is used to identify the beam particle. Fig. 2 illustrates the beam composition measured with these two quantities. The y-axis shows the calibrated time-of-flight from the A-S1 system with the nuclei with $A = 2Z$ at 0.0 ps while $A > 2Z$ and $A < 2Z$ nuclei are placed above and below this line respectively. The beam trigger was set to $Z = 6$, and ^{12}C nuclei were selected by making an offline cut on the time-of-flight. We use polyethylene (C_2H_4 , hereafter called PE) as our main proton target, a graphite (C) target to account for C+C interactions in the PE target and about 10% of the total events are recorded with an empty target holder to measure the interaction of the beam outside the target. The magnetic field scale factor of the vertex magnets was set to 59% of the full-field value 9 Tm. This value was selected as the optimal \vec{B} -field such that the beam and its fragmented counterparts deflect into the MTPC, minimizing any beam interactions in the TPC support structures downstream of the target.

The fragments produced in the beam-target interaction are deflected w.r.t. to the nominal beam position ($\Delta x = x_{\text{frag}} - x_{\text{beam}}$) in the magnetic field on their way to the MTPC-L, subject to change in their rigidity relative to the beam rigidity. The energy deposit dE/dx in the MTPC is a direct measure of the charge of the fragment. These two pieces of information are used to identify the element and its corresponding isotope. The distribution of fragments in the MTPC is shown in Fig. 3 for the target IN and OUT cases, with $A/Z = 2$ particles at $\Delta x = 0.0$ cm. In order to

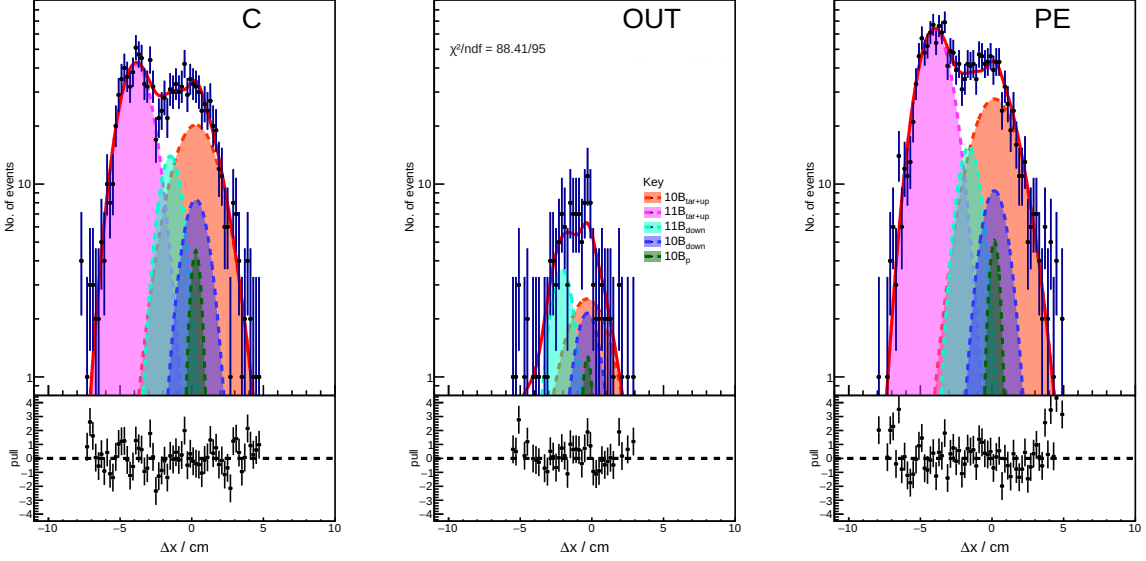


Figure 4: Fit results to the Δx -distribution of boron fragments in the MTPC for the three target settings. The fit peaks are the ^{11}B (pink) & ^{10}B (orange) produced upstream and in the target. While the ^{11}B (cyan) & ^{10}B (blue) are the resultant fragments from the downstream interaction of the beam. The narrow green peak depicts the fractional primary ^{10}B component resulting from the beam-selection cuts.

ensure that only the boron fragments produced from the beam-target interactions are measured in the MTPC, we place re-interaction cuts on Z^2 of the preceding TPCs, such as $Z_{\text{TPC}}^2 < 33.0$ & $Z_{\text{VTPC2}}^2 < 31.0$. Moreover for boron selection in the MTPC, only tracks with more than 70 clusters that satisfy the following charge cut: $22.5 \leq Z_{\text{MTPC}}^2 \leq 27.5$ are selected for the final analysis. The Δx -distribution of the measured boron fragments for the three target settings are shown in Fig. 4. A fit to the three data sets is performed to retrieve the isotopic yields of ^{10}B & ^{11}B . A flat-top Gaussian function is used to model the detector response. It is a result of the convolution of a rectangular box function to model the momentum acceptance of the beam, $\Delta p/p \approx 1\%$, and a normalized Gaussian function to describe the Δx track resolution of the MTPC. Furthermore, the fragmentation process introduces a non-zero component of the Fermi momentum in the rest frame which when boosted to the laboratory frame through the magnetic field, induces a spatial spread in the fragment peaks (hereafter called the Fermi width). This is taken into account by convolving a Gaussian function with the detector model.

We perform a combined fit simultaneously to all three data sets (viz. PE, C & OUT), in which the detector model parameters and the Fermi widths of the fragments are shared amongst the data sets. While the isotopic yields of the signal ^{11}B (pink peak in Fig. 4) & ^{10}B (orange peak in Fig. 4) are determined by normalization of each of the fit peaks for every data set.

3.2 Computing Isotopic Production Cross-sections

The main goal of this work is to measure the production cross-sections of ^{10}B & ^{11}B in $^{12}\text{C}+p$ interactions. The isotopic yields retrieved from the fit described in Section 3.1 are used to compute the production probability. We divide the experiment into roughly 3 regions called the upstream (up) comprising the beam detectors before the target, the target itself (T), and the downstream (dn)

region which includes the TPCs and the experimental support structures. In the following analysis, the beam nuclei are denoted with the short-form ‘b’ whereas the produced fragment of interest is denoted by ‘f’. The corresponding production probability is written with the subscript $b \rightarrow f$ whereas the probability that a nucleus retains its identity, called the survival probability is written with the subscript $b \rightarrow b$ for the beam and similarly $f \rightarrow f$ for the fragment nucleus. With these notations defined, the total measured production probability of ^{11}B from the ^{12}C beam interactions (orange peak in Fig. 4) is written as follows,

$$P^{\text{tot,IN}} = P_{b \rightarrow f}^{\text{up}} P_{f \rightarrow f}^{\text{T}} P_{f \rightarrow f}^{\text{dn}} + P_{b \rightarrow b}^{\text{up}} P_{b \rightarrow f}^{\text{T}} P_{f \rightarrow f}^{\text{dn}}. \quad (1)$$

The first term gives the upstream production while the second term is the production of ^{11}B from the target. ^{11}B produced downstream of the target (cyan peak in Fig. 4) does not interfere with the signal and hence is not considered in the above equation. Similarly for the OUT case, since there is no contribution from the target, $P_{b \rightarrow f}^{\text{T}} = 0$ while the target survival term, $P_{f \rightarrow f}^{\text{T}} = 1$, the total measured probability is written as the following expression,

$$P^{\text{tot,OUT}} = P_{b \rightarrow f}^{\text{up}} P_{f \rightarrow f}^{\text{dn}}. \quad (2)$$

Therefore, by dividing Eq. (1) by Eq. (2), we can solve for the in-target production probability of ^{11}B to obtain the following equation,

$$\frac{P^{\text{tot,IN}}}{P^{\text{tot,OUT}}} = P_{f \rightarrow f}^{\text{T}} + \frac{P_{b \rightarrow b}^{\text{up}}}{P_{b \rightarrow f}^{\text{up}}} P_{b \rightarrow f}^{\text{T}}. \quad (3)$$

It is interesting to note that all the quantities in Eq. (3) are directly measurable except for the ratio in the second term on the right. The first term is the target survival probability of ‘f’ and is simply written as the ratio of the total measured in-elastic probability for the IN and the OUT case, as, $P_{f \rightarrow f}^{\text{tot,IN}}/P_{f \rightarrow f}^{\text{tot,OUT}}$. It is noteworthy that this fragment nucleus is already present in the data which enables us to make this auxiliary measurement by altering the upstream cuts to select nucleus ‘f’ as the primary beam particle. Now, the second term is the ratio of the upstream probabilities. This probability too can be estimated from auxiliary measurements of nucleus ‘f’. Ultimately, after making the appropriate substitutions, Eq. (3) can be solved for the in-target production probability $P_{b \rightarrow f}^{\text{T}}$. The final expression is written as follows,

$$P_{b \rightarrow f}^{\text{T}} = \frac{P_{f \rightarrow f}^{\text{up}}}{P_{b \rightarrow b}^{\text{up}}} \frac{1}{P_{f \rightarrow f}^{\text{tot,OUT}}} \left(P_{b \rightarrow f}^{\text{tot,IN}} - P_{b \rightarrow f}^{\text{tot,OUT}} - P_{f \rightarrow f}^{\text{tot,OUT}} P_{f \rightarrow f}^{\text{T}} \right). \quad (4)$$

A significant and largest component to the upstream material budget arises from the contribution of the S1 detector and hence is the most probable location for the beam to interact. It is a 0.5 cm thick scintillator made up of polyvinyl-toluene. Thus the leading ratio can be estimated from the in-elastic cross-sections for ‘b’ & ‘f’ nuclei with the PE target and scaled to the C:H ratio of the S1 material. This value evaluates to ~ 1 , and hence simplifies our calculation.

In the case of cross-section calculation for ^{10}B , there are two additional contributions to the signal from the ^{11}C & ^{11}B which are produced in the upstream fragmentation of the ^{12}C beam. These nuclei can interact with the target to produce ^{10}B and add to the total measured ^{10}B in the

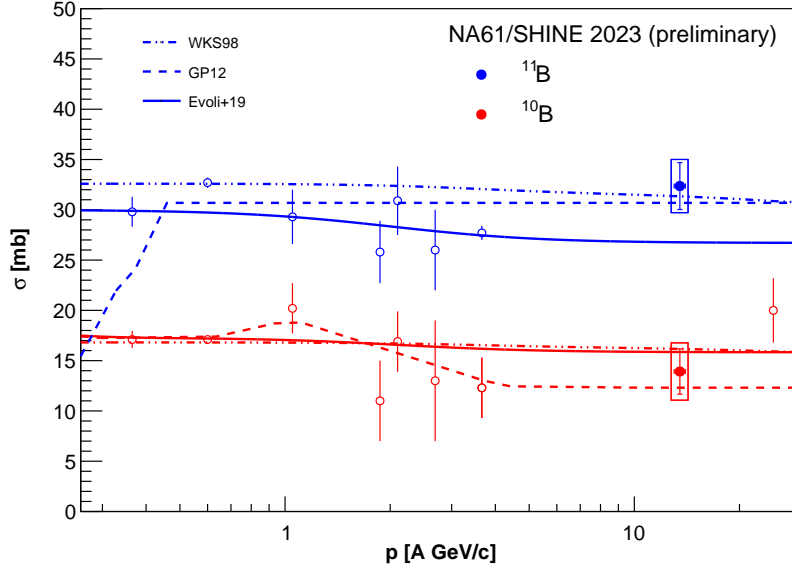


Figure 5: Preliminary NA61/SHINE measurement (solid markers) of the production of boron isotopes ^{11}B (blue) & ^{10}B (red) compared to previous measurements (open markers) [11–16]. The total uncertainty (stat.+syst.) for each measurement is shown by the box whereas the line gives the statistical uncertainty.

MTPC (*orange* peak in Fig. 4). But since these interactions are $O(P^2)$ and since $P \ll 1$, such two-step reactions can be safely ignored in the analysis. Therefore, an approach exactly like the ^{11}B analysis detailed above can be used for ^{10}B as well.

The production cross-section from a target (T) can be computed as,

$$\sigma^{\text{T}} = -\frac{M_{\text{T}}}{N_{\text{A}} \rho_{\text{T}} d_{\text{T}}} \ln(1 - P_{\text{b} \rightarrow \text{f}}^{\text{T}}). \quad (5)$$

Here, M_{T} is the molar mass, ρ_{T} the density and d_{T} is the thickness of the target and N_{A} is Avogadro's constant. Finally, the $^{12}\text{C}+\text{p}$ cross-section can be calculated by subtracting the cross-sections for PE & C targets and dividing by 2. Thus the final expression for the production cross-section of a fragment 'f' is written as,

$$\sigma_{^{12}\text{C} \rightarrow \text{f}}^{\text{p}} = \frac{1}{2}(\sigma_{^{12}\text{C} \rightarrow \text{f}}^{\text{PE}} - \sigma_{^{12}\text{C} \rightarrow \text{f}}^{\text{C}}). \quad (6)$$

The factor 1/2 comes from the fact that the ratio C : H = 1 : 2 in every polymer cell of the PE target.

4. Results and Conclusion

The measured production probability is further subject to corrections which also induce a systematic uncertainty. For instance, the systematic uncertainty due to the loss of the boron signal due to the inelastic interaction of the produced fragment before exiting the target. This is computed using the measured in-elastic interaction probability of the fragment nuclei as the primary beam particle. Thus systematic error due to this correction is actually dominated by statistics. Additional corrections applied are feed-down from beam impurity nuclei and charge selection of the fragment tracks in the MTPC.

The preliminary measurement of production cross-sections for the two boron isotopes is,

$$\sigma_{12\text{C}\rightarrow^{10}\text{B}}^{\text{P}} = (13.9 \pm 2.2 \text{ (stat.)} \pm 1.8 \text{ (syst.)}) \text{ mb}, \quad (7)$$

$$\sigma_{12\text{C}\rightarrow^{11}\text{B}}^{\text{P}} = (32.3 \pm 2.3 \text{ (stat.)} \pm 1.3 \text{ (syst.)}) \text{ mb}. \quad (8)$$

Our results are in good agreement compared to the previous measurements [11–16] and model lines, shown in Fig. 5. The lines depict different parameterizations of the cross-section as a function of p/A corresponding to GALPROP12 [17], WKS98 (see Ref. [5],[18–20]) and Evoli+19 [21]. It is interesting to note that there is only one measurement of the production cross-sections of boron isotopes at $p > 10A$ GeV/ c by [11]. The reported cross-section for ^{11}B is (59 ± 12) mb and that for ^{10}B is (20 ± 3) mb at $p = 25A$ GeV/ c and corresponds to the cumulative value including contribution from ^{11}C and ^{10}C respectively. Combining our current result with the previously reported ^{11}C cross-section measurement [8] will be crucial in determining the total boron production in the Galaxy. Moreover, the future data-taking runs at NA61/SHINE will enable us to study the fragmentation of various primary nuclei like C, N, O, up to Si into lighter nuclei, with higher statistics and improved precision.

Acknowledgement

We would like to thank the organizers for the opportunity to present our results at this conference, ICRC23. The fragmentation measurements are supported by the NCN-DFG Beethoven CLASSIC 3 funding of the Deutsche Forschungsgemeinschaft (DFG – German Research Foundation) project number 426579465 and the Polish Ministry of Science and Higher Education grant 2018/31/G/ST2/03910.

References

- [1] O. Adriani *et al.* [PAMELA Collab.], *Astrophys. J.* **791** (2014) 93.
- [2] M. Aguilar *et al.* [AMS Collab.], *Phys. Rev. Lett.* **117** (2016) 231102.
- [3] O. Adriani *et al.* [CALET Collab.], *Phys. Rev. Lett.* **129** (2022) 251103.
- [4] F. Alemanno *et al.* [DAMPE Collab.], *Sci. Bull.* **67** (2022) 2162.
- [5] Y. Genolini *et al.*, *Phys. Rev. C* **98** (2018) 034611.
- [6] Y. Genolini *et al.*, [arXiv:2307.06798](https://arxiv.org/abs/2307.06798).
- [7] M. Unger [NA61/SHINE Collab.], PoS(ICRC2019)446 [arXiv:1909.07136](https://arxiv.org/abs/1909.07136).
- [8] N. Amin [NA61/SHINE Collab.], PoS(ICRC2021)102 [arXiv:2107.12275](https://arxiv.org/abs/2107.12275).
- [9] N. Abgrall *et al.* [NA61/SHINE Collab.], *JINST* **9** (2014) P06005.
- [10] A. Aduszkiewicz *et al.* [NA61/SHINE Collab.], SPSC-P-330-ADD-9, CERN-SPSC-2017-035.
- [11] P. Fontes, *Phys. Rev. C* **15** (1977) 2159.
- [12] A. Korejwo *et al.*, *Proc. 26th ICRC*, **4** (1999) 267.
- [13] A. Korejwo *et al.*, *J. Phys. G Nucl. Phys.* **28** (2002) 1199.
- [14] D.L. Olson *et al.*, *Phys. Rev. C* **28** (1983) 1602.
- [15] W.R. Webber, *AIP Conf. Proc.* **203** (1990) 294.
- [16] W.R. Webber, *et al.*, *Phys. Rev. C* **41** (1990) 533.
- [17] W.R. Webber *et al.*, *Phys. Rev. C* **41** (1990) 566
- [18] W.R. Webber *et al.*, *Phys. Rev. C* **58** (1998) 3539
- [19] W.R. Webber *et al.*, *Phys. Rev. C* **508** (1998) 940
- [20] W.R. Webber, *et al.*, *Phys. Rev. C* **508** (1998) 949
- [21] C. Evoli, R. Aloisio, P. Blasi, *Phys. Rev. D* **99** (2019) 103023.

The NA61/SHINE Collaboration



H. Adhikary ¹³, P. Adrich ¹⁵, K.K. Allison ²⁶, N. Amin ⁵, E.V. Andronov ²², T. Antićić ³, I.-C. Arsene ¹², M. Bajda ¹⁶, Y. Balkova ¹⁸, M. Baszczyk ¹⁷, D. Battaglia ²⁵, A. Bazgir ¹³, S. Bhosale ¹⁴, M. Bielewicz ¹⁵, A. Blondel ⁴, M. Bogomilov ², Y. Bondar ¹³, A. Brandin ²², W. Bryliński ²¹, J. Brzychczyk ¹⁶, M. Buryakov ²², A.F. Camino ²⁸, M. Čirković ²³, M. Csanád ⁸, J. Cybowska ²¹, T. Czopowicz ¹³, C. Dalmazzone ⁴, N. Davis ¹⁴, A. Dmitriev ²², P. von Doetinchem ²⁷, W. Dominik ¹⁹, P. Dorosz ¹⁷, J. Dumarchez ⁴, R. Engel ⁵, G.A. Feofilov ²², L. Fields ²⁵, Z. Fodor ^{7,20}, M. Friend ⁹, M. Gaździcki ^{13,6}, O. Golosov ²², V. Golovatyuk ²², M. Golubeva ²², K. Grebieszkow ²¹, F. Guber ²², S.N. Igolkin ²², S. Ilieva ², A. Ivashkin ²², A. Izvestnyy ²², K. Kadija ³, N. Kargin ²², N. Karpushkin ²², E. Kashirin ²², M. Kielbowicz ¹⁴, V.A. Kireyeu ²², R. Kolesnikov ²², D. Kolev ², Y. Koshio ¹⁰, V.N. Kovalenko ²², S. Kowalski ¹⁸, B. Kozłowski ²¹, A. Krasnoperov ²², W. Kucewicz ¹⁷, M. Kuchowicz ²⁰, M. Kuich ¹⁹, A. Kurepin ²², A. László ⁷, M. Lewicki ²⁰, G. Lykasov ²², V.V. Lyubushkin ²², M. Maćkowiak-Pawłowska ²¹, Z. Majka ¹⁶, A. Makhnev ²², B. Maksiak ¹⁵, A.I. Malakhov ²², A. Marcinek ¹⁴, A.D. Marino ²⁶, H.-J. Mathes ⁵, T. Matulewicz ¹⁹, V. Matveev ²², G.L. Melkumov ²², A. Merzlaya ¹², Ł. Mik ¹⁷, A. Morawiec ¹⁶, S. Morozov ²², Y. Nagai ⁸, T. Nakadaira ⁹, M. Naskręt ²⁰, S. Nishimori ⁹, A. Olivier ²⁵, V. Ozvenchuk ¹⁴, O. Panova ¹³, V. Paolone ²⁸, O. Petukhov ²², I. Pidhurskyi ^{13,6}, R. Płaneta ¹⁶, P. Podlaski ¹⁹, B.A. Popov ^{22,4}, B. Pórfy ^{7,8}, M. Posiała-Zezula ¹⁹, D.S. Prokhorova ²², D. Pszczel ¹⁵, S. Puławski ¹⁸, J. Puzović ^{23†}, R. Renfordt ¹⁸, L. Ren ²⁶, V.Z. Reyna Ortiz ¹³, D. Röhrich ¹¹, E. Rondio ¹⁵, M. Roth ⁵, Ł. Rozpłochowski ¹⁴, B.T. Rumberger ²⁶, M. Rumyantsev ²², A. Rustamov ^{1,6}, M. Rybczynski ¹³, A. Rybicki ¹⁴, K. Sakashita ⁹, K. Schmidt ¹⁸, A.Yu. Seryakov ²², P. Seyboth ¹³, U.A. Shah ¹³, Y. Shiraishi ¹⁰, A. Shukla ²⁷, M. Słodkowski ²¹, P. Staszal ¹⁶, G. Stefanek ¹³, J. Stepaniak ¹⁵, M. Strikhanov ²², H. Ströbele ⁶, T. Šušar ³, Ł. Świdorski ¹⁵, J. Szewiński ¹⁵, R. Szukiewicz ²⁰, A. Taranenko ²², A. Tefelska ²¹, D. Tefelski ²¹, V. Tereshchenko ²², A. Toia ⁶, R. Tsenov ², L. Turko ²⁰, T.S. Tveter ¹², M. Unger ⁵, M. Urbaniak ¹⁸, F.F. Valiev ²², D. Veberič ⁵, V.V. Vechernin ²², V. Volkov ²², A. Wickremasinghe ²⁴, K. Wójcik ¹⁸, O. Wyszłyński ¹³, A. Zaitsev ²², E.D. Zimmerman ²⁶, A. Zwiagina ²², and R. Zwaska ²⁴

[†] deceased

¹ National Nuclear Research Center, Baku, Azerbaijan

² Faculty of Physics, University of Sofia, Sofia, Bulgaria

³ Ruđer Bošković Institute, Zagreb, Croatia

⁴ LPNHE, Sorbonne University, CNRS/IN2P3, Paris, France

⁵ Karlsruhe Institute of Technology, Karlsruhe, Germany

⁶ University of Frankfurt, Frankfurt, Germany

⁷ Wigner Research Centre for Physics, Budapest, Hungary

⁸ Eötvös Loránd University, Budapest, Hungary

⁹ Institute for Particle and Nuclear Studies, Tsukuba, Japan

¹⁰ Okayama University, Japan

¹¹ University of Bergen, Bergen, Norway

¹² University of Oslo, Oslo, Norway

¹³ Jan Kochanowski University, Kielce, Poland

¹⁴ Institute of Nuclear Physics, Polish Academy of Sciences, Cracow, Poland

¹⁵ National Centre for Nuclear Research, Warsaw, Poland

- ¹⁶ Jagiellonian University, Cracow, Poland
- ¹⁷ AGH - University of Science and Technology, Cracow, Poland
- ¹⁸ University of Silesia, Katowice, Poland
- ¹⁹ University of Warsaw, Warsaw, Poland
- ²⁰ University of Wrocław, Wrocław, Poland
- ²¹ Warsaw University of Technology, Warsaw, Poland
- ²² Affiliated with an institution covered by a cooperation agreement with CERN
- ²³ University of Belgrade, Belgrade, Serbia
- ²⁴ Fermilab, Batavia, USA
- ²⁵ University of Notre Dame, Notre Dame, USA
- ²⁶ University of Colorado, Boulder, USA
- ²⁷ University of Hawaii at Manoa, Honolulu, USA
- ²⁸ University of Pittsburgh, Pittsburgh, USA